JCTC Journal of Chemical Theory and Computation

Article

pubs.acs.org/JCTC

Diatomics-in-Molecules Modeling of Many-Body Effects on the Structure and Thermodynamics of Mercury Clusters

F. Calvo,*[,†] E. Pahl,[‡] P. Schwerdtfeger,[§] and F. Spiegelman[∥]

[†]LASIM, CNRS UMR 5579, Université de Lyon, 43 Bd. du 11 Novembre 1918, F69622 Villeurbanne Cedex, France

[‡]Centre for Theoretical Chemistry and Physics, Institute of Natural Science, Massey University Albany, Private Bag 102904, North Shore City, 0745 Auckland, New Zealand

[§]Centre for Theoretical Chemistry and Physics, New Zealand Institute for Advanced Study, Massey University Albany, Private Bag 102904, North Shore City, 0745 Auckland, New Zealand and Fachbereich Chemie, Philipps-Universität Marburg, Hans-Meerwein-Str. D35032 Marburg, Germany

[∥]LCPQ, CNRS and Université de Toulouse (UPS), 118 Route de Narbonne, F31062 Toulouse Cedex, France

Supporting Information

ABSTRACT: The stable structures and melting behavior of Hg_n clusters, $2 \leq n < 60$, have been theoretically investigated using an updated diatomics-in-molecules (DIM) model initially proposed by Kitamura [*Chem. Phys. Lett.* **2006**, *425*, 2056]. Global optimization and sampling at finite temperature are achieved on the basis of hierarchical and nested Markov chain Monte Carlo methods, respectively. The DIM model predicts highly symmetric icosahedral global minima that are generally similar to the standard van der Waals atomic clusters, without any indication of distorted or low-coordinated geometries, but also at variance with the global minima found with the pairwise Hg_2 potential. The combined influences of surface and many-body effects due to s−p mixing are considerable on the melting point: although the model predicts a bulk melting temperature in fair agreement with experimental results, it is found to decrease with increasing cluster size.

1. INTRODUCTION

Mercury shows very peculiar properties in the bulk phases.[1] Its normal crystal structure is rhombohedral instead of the hexagonal close-packed structure of other group 12 elements.[2] Besides being the only liquid metal at room temperature, it also has the lowest critical temperature of all metals, making it especially attractive for experimental studies of the liquid and vapor states.[3,4] Upon reaching the critical point, the electrical conductivity decreases and the metallic character is lost. This has led to a wealth of theoretical studies aimed at unraveling the interatomic potentials that could account for the observed fluid structure.[5−7] The vapor state also exhibits dielectric anomalies[8] and excimer formation that could enhance nucleation rates.[9]

In addition to changing the fluid density, the metal to nonmetal transition in mercury can be triggered by varying the number of atoms in a cluster.[10] After the first evidence that small Hg clusters are indeed nonmetallic,[11] successive experiments over recent decades have addressed this issue using synchrotron,[12] laser,[13,14] photoelectron,[15,16] and photoionization[17] spectroscopies. Mass spectrometry has been used by several groups to characterize size stabilities of multiply charged clusters.[18,19] More recently, kinetic map imaging[21] and excited states dynamics have been investigated.[20−22] Nevertheless, the size ranges at which Hg clusters become semiconducting, then metallic, are still under debate, notably because different properties such as ionization potential or electronic band gap may be related differently to the progression in metallic character.

Not surprisingly, the intriguing metal to nonmetal transition in mercury has motivated a large number of theoretical studies as well, in relation with bulk[23−26] and clusters.[27−37] From these studies, the chemical and physical peculiarities of mercury are generally ascribed both to the alkaline earth nature of this metal and to relativistic effects,[38,39] which in particular stabilize the 6s band to a significant amount. Unfortunately, the interactions in mercury systems are notoriously difficult to calculate:[40] while DFT may lack accuracy for mercury,[42,43] a many-body expansion of the potential converges slowly, if at all.[41,42] A possible solution is to describe only the electron correlation by its pairwise contribution and add the mean field (Hartree−Fock) energy of the whole system.[41,42]

As an alternative to first-principle theoretical chemistry approaches, a simple quantum model was proposed by Kitamura,[45] who suggested representing the many-body effects due to s−p mixing in small clusters by means of the diatomics-in-molecules (DIM) approximation.[46−50] Although based on *ab initio* ingredients for atomic and diatomic fragments only, the DIM model was found to reproduce the binding energies of Hg_n aggregates containing up to seven atoms, as predicted by electronic structure calculations at the CCSD(T) level.[37] The success of the method was then exploited by Kitamura to relate the many-body contribution to the binding energy with the coordination number in a semiempirical evaluation of the coexistence curve of liquid mercury.[51]

The DIM formalism developed by Kitamura is appealing from the theoretical perspective, because it is based on a simplified Hamiltonian, with well-controlled approximations

Received: November 23, 2011
Published: January 27, 2012

involving the most important chemical features of van der Waals interactions, s−p mixing, and spin−orbit couplings. It is intrinsically many-body, and the diatomic inputs can be accurately determined today via *ab initio* calculations. The Kitamura formulation allows a relatively easy evaluation of the importance of many-body effects resulting from the DIM tensorial couplings. From the computational point of view, it is also practical enough to make systematic sampling issues such as unbiased global optimization or molecular simulation tractable even for relatively large systems.

In the present work, we have used the DIM approach to investigate the stable structures of neutral Hg_n clusters. The cluster sizes considered here remain in the nonmetallic domain, for which the DIM method is expected to give reasonable results. Direct ($n \leq 30$) and hierarchical ($30 < n < 60$) global optimization methods were employed to locate the most stable geometries, and our results generally indicate that the usual icosahedral motifs associated with atomic van der Waals clusters are also present for mercury, albeit with some unexpected 6-fold symmetry elements not reported so far.

We are also interested in the thermodynamical behavior, in relation with the melting phase change. Due to the evolution of chemical bonding with increasing cluster size, we do not anticipate that scaling laws, such as those found in the melting point of rare-gas,[52] noble,[53] or transition[54] metals, also exist for mercury. However, it is unclear how the increasingly delocalized electronic wave function will impact the thermal stability of small clusters as they progressively leave the insulating regime. For the purpose of evaluating thermodynamical properties, and contrary to the phenomenological approach of ref 51, we have pursued a more direct sampling strategy of the energy landscapes of selected cluster sizes. However, the substantial computational effort associated with solving the eigenproblem of the DIM Hamiltonian for each configuration could be significantly reduced by means of auxiliary potentials obtained by first-order perturbation theory, along lines previously laid in the context of tight-binding Hamiltonians.[55] The auxiliary potential technique,[56,57] also known as nested Markov Chain Monte Carlo [N(MC)^2], is here rigorously combined with the parallel tempering strategy[58,59] in order to achieve efficient and hopefully ergodic exploration of the energy landscape of clusters having up to 55 atoms. These simulations with the DIM model predict an unexpected *lowering* in the melting temperature for increasing cluster size, which is mostly due to the many-body contribution to potential energy, still under a strong influence of surface effects.

The paper is organized as follows. In the next section, we briefly present the DIM model and the methods used to perform global optimization and sampling at finite temperature, including the details of our implementation of nested Markov Chain parallel tempering Monte Carlo. The structural results are given and discussed in section 3, and the melting behavior is the subject of section 4. We finally give some concluding remarks and draw some perspectives in section 5.

2. METHODS

This section successively describes the model used to represent the ground electronic state, the global optimization strategies, and the Monte Carlo methodology employed to sample the potential energy surfaces at nonzero temperatures.

2.1. DIM Model. The diatomics-in-molecules method was laid out decades ago by Ellison, Kuntz, and others as an approximation at the level of configuration interaction (CI) theory, in which the CI matrix is expressed in a valence-bond many-electron basis, the matrix elements being those of the diatomic building pairs.[46−50] For mercury clusters, the method has been developed to incorporate the mixing effects of 6p orbitals into the 6s state arising between ground and excited states of the same $^1\Sigma_g^+$ symmetry.

The electronic state of an n-atom mercury cluster with configuration **R** is described by a linear combination of many-body functions written as a product of localized atomic wave functions, which do not overlap. Spin−orbit couplings are accounted for by their individual atomic contribution. The directional dependence associated with p orbitals is incorporated by suitable rotation of the electronic wave function between the diatomic and laboratory frames.

In the presence of spin−orbit coupling, the 9-fold and 3-fold degeneracies of atomic Hg(6s6p^{3}P) and Hg(6s6p^{1}P) impose 12 basis functions per atom to describe the excited states, the product functions being constructed with all but one of the atoms in their ground states. Spin−orbit coupling is introduced via its atomic contribution between the atomic configurations of the 6s6p configurations, as proposed by Cohen and Schneider[60] for rare gases. Taking into account the product function where all atoms are in the ground state leads to a Hamiltonian described by a $(12n + 1)$-square Hermitian matrix, in which all elements are related via simple combinations of the diatomic potential energy curves for the ground state $X^1\Sigma_g^+$ and the excited states $^3\Sigma_g^+$, $^3\Sigma_u^+$, $^3\Pi_g$, $^3\Pi_u$, $^1\Sigma_g^+$, $^1\Sigma_u^+$, $^1\Pi_g$, and $^1\Pi_u$. Spin−orbit matrix elements are described by the superposition of atomic contributions, neglecting any dependence on geometry. By construction, the DIM method exactly gives the correct ground and excited states used as inputs for the dimer.

The computational details, including all expressions for the mixing coefficients $\xi(r)$ between the $X^1\Sigma_g^+$ and $^1\Sigma_g^+$ states and the overall Hamiltonian matrix, are those detailed by Kitamura.[45] However, in contrast with the original work, parametric functions were used to represent the excited energy curves of Hg_2 obtained by Czuchaj and co-workers at the MRCI and SCF levels.[61] Purely repulsive excited states were represented on the basis of the following expression:

$$V(^{2S+1}\Lambda, r) = D \exp(-ar) + c_S \frac{C_3}{r^3} \tag{1}$$

with S being the spin state and the parameters, all given in atomic units, being $D = 13.66898$, $a = 1.2$, $c_S = 2$, and $C_3 = 4.6825$ for $^1\Sigma_g^+$; $D = 12.434$, $a = 0.988$, and $C_3 = 0$ for $^3\Sigma_g^+$; $D = 104.795$, $a = 1.6$, $c_S = 1$, and $C_3 = 4.6825$ for $^1\Pi_u$; and $D = 1085.52$, $a = 2.196$, and $C_3 = 0$ for $^3\Pi_u$. The C_3 term is primarily related to dipole−dipole interactions and is responsible for excitation transfer.

A Morse oscillator is used for the other excited states states as

$$V(^{2S+1}\Lambda, r) = D\{\exp[-2a(r - r_e)] - 2\exp[-a(r - r_e)]\} - c_S \frac{C_3}{r^3} \tag{2}$$

with $D = 0.0189$, $a = 0.85$, $r_e = 5.5$, $c_S = 2$, and $C_3 = 7.477$ for $^1\Sigma_u^+$; $D = 0.0368$, $a = 0.8$, $r_e = 5.37$, and $C_3 = 0$ for $^3\Sigma_u^+$; $D = 0.065611$, $a = 0.77$, $r_e = 5.1$, $c_S = 1$, and $C_3 = 2.81$ for $^1\Pi_g$; and $D = 0.04697$, $a = 0.87$, $r_e = 5.14$, and $C_3 = 0$ for $^3\Pi_g$. In addition, the ground state energy curve was also updated to a more

dx.doi.org/10.1021/ct200846a | J. Chem. TheoryComput. 2012, 8, 639−648

accurate extended Lennard-Jones (LJ) form:

$$V(X^1\Sigma_g^+, r) = \sum_{k=1}^{9} \frac{a_k}{r^{k+5}} \tag{3}$$

with parameters a_k optimized to reproduce recent CCSD(T) calculations.[62] Except for these diatomic ingredients, all other parametric functions for the mixing and atomic contributions were taken exactly as those of ref 45.

Once all matrix elements are calculated, the eigenproblem is solved, and the lowest eigenvalue provides the ground electronic state of the cluster including by s−p mixing, which is henceforth denoted as $V_{\mathrm{DIM}}(\mathbf{R})$. Note that the reference surface is also chosen in such a way that the potential vanishes at infinite atomic separation. Canceling the mixing term ($\xi = 0$) leads to a purely classical potential $V_{\mathrm{pair}}(\mathbf{R})$ that is the sum of eq 3 over all pairs of atoms, also vanishing asymptotically.

2.2. Global Optimization. The stable structures of mercury clusters were located using systematic global optimization methods based on basin-hopping Monte Carlo.[63,64] As with genetic algorithms, this powerful method makes extensive use of local optimizations starting from randomly perturbed geometries. In the DIM methodology, the gradient is analytic but rather cumbersome and computationally costly, especially considering that the energy evaluation already involves solving the eigenproblem for a $(12n + 1)^2$ Hermitian matrix. The numerical gradient, on the other hand, can be rather cheap owing to first-order perturbation theory.

Denoting $|\Psi_0(\mathbf{R})\rangle$ the ground state eigenvector obtained at a reference configuration $\mathbf{R}$, and assuming the eigenvectors are normalized, the energy $E + \Delta E$ associated with a small change $\delta\mathbf{R}$ in coordinates is simply given by

$$E + \Delta E \simeq \langle\Psi_0(\mathbf{R})|H(\mathbf{R} + \delta\mathbf{R})|\Psi_0(\mathbf{R})\rangle \tag{4}$$

which in the following is by definition referred to as $E + \Delta E = V_{\mathrm{pert}}(\mathbf{R} + \delta\mathbf{R})$. Once the eigenproblem is solved for configuration $\mathbf{R}$, moving one atom at a time only changes very few elements in the Hamiltonian matrix, making the evaluation of the above equation scale linearly with n. The net computational cost for evaluating the numerical gradient for all coordinates thus scales as n^2, rather than n^3 for the analytic gradient. In addition, the small atomic displacements required for an accurate evaluation of the numerical gradient also make the perturbation formula more accurate. In practice, we have used $\delta R = 10^{-5}$ bohr for each atomic Cartesian coordinate.

Basin-hopping global minimization was undertaken to locate the lowest-energy structures of Hg_n clusters with $n \leq 30$. For each cluster size, five series of 10^4 quenches were performed after random collective moves with large amplitude δR = 2.5 bohr, the new configuration being accepted or rejected according to a Metropolis criterion evaluated at T = 300 K.

Above 30 atoms, the computational cost of the DIM model and the gradient became too high, and we turned to a semiglobal optimization method, in which large databases of minima are generated by basin-hopping Monte Carlo but for the much simpler pairwise model in the absence of s−p mixing. Each minimum is then locally optimized using the full many-body potential $V_{\mathrm{DIM}}(\mathbf{R})$, and the lowest-energy minimum is identified from this optimized set.[65]

2.3. Sampling at Finite Temperature. One of our ultimate goals in the study of mercury clusters is to determine their thermodynamical behavior as they change from van der Waals to covalent and metallic binding. Computing thermodynamical indicators such as caloric curves requires extensive sampling of the potential energy landscapes, which in the present work was achieved using Monte Carlo techniques at finite temperature.

For relatively expensive potential energy surfaces, it is advantageous to consider approximate representations (an auxiliary potential) to accelerate the sampling. The flexibility of MC methods allows such approximate schemes to be carried out rigorously, correcting periodically the deviations to the reference energy surface. The nested Markov chain Monte Carlo method used here was independently proposed by several groups[56,57] and shown to be particularly efficient in bulk[66] and cluster[67] simulations in various statistical ensembles.

Briefly, we denote by T the fixed temperature, by $\beta = 1/k_{\mathrm{B}}T$ its inverse (with k_{B} the Boltzmann constant), and by $V_{\mathrm{approx}}(\mathbf{R})$ an approximation to the reference DIM potential energy surface $V_{\mathrm{DIM}}(\mathbf{R})$ we wish to sample. At the current configuration $\mathbf{R}_i$, a number M of elementary random MC steps are performed, $\mathbf{R}_i \rightarrow \mathbf{R}_{i+1} \rightarrow \cdots \rightarrow \mathbf{R}_{i+M}$, and accepted on the basis of a Metropolis criterion with the approximate energy surface V_{approx}. The configuration $\mathbf{R}_{i+M}$ is then tested against the original potential surface V_{DIM}, and it is accepted in the sample of the reference system on the basis of a combined Metropolis probability as[56,57]

$$\mathrm{acc}(\mathbf{R}_i \rightarrow \mathbf{R}_{i+M}) = \min\left\{1, \frac{\exp(-\beta[V_{\mathrm{DIM}}(\mathbf{R}_{i+M}) - V_{\mathrm{DIM}}(\mathbf{R}_i)])}{\exp(-\beta[V_{\mathrm{approx}}(\mathbf{R}_{i+M}) - V_{\mathrm{approx}}(\mathbf{R}_i)])}\right\} \tag{5}$$

In case of rejection, the entire Markov chain leading from $\mathbf{R}_i$ to $\mathbf{R}_{i+M}$ on the approximate surface is discarded, and $\mathbf{R}_i$ is copied as $\mathbf{R}_{i+M}$. Statistical averages and distributions on the reference surface V_{DIM} can then be taken as usual, every M steps. The proximity between the two potentials is of course a key factor in increasing the acceptance probability of eq 5. The global efficiency of the N(MC)^2 method is then mostly limited by this proximity and the computational gain of replacing the reference potential by its approximation, and by the value of M, which should be taken to be as large as possible, still keeping the drift of V_{approx} relative to V_{DIM} within reason.[67]

A natural approximate surface can be designed for the DIM potential by considering for $V_{\mathrm{approx}}(\mathbf{R})$ the first-order perturbed potential of eq 4 defined with respect to the reference configuration $\mathbf{R}_i$. By definition, this auxiliary potential $V_{\mathrm{pert}}(\mathbf{R})$ equals the reference energy surface for $\mathbf{R}_i$; hence the Metropolis acceptance rate simplifies as

$$\mathrm{acc}(\mathbf{R}_i \rightarrow \mathbf{R}_{i+M}) = \min\{1, \exp(-\beta[V_{\mathrm{DIM}}(\mathbf{R}_{i+M}) - V_{\mathrm{pert}}(\mathbf{R}_{i+M})])\} \tag{6}$$

and is thus fully controlled by the extent of the drift of the first-order perturbation method. Adjusting the size step on the approximate surface to get about a 50% acceptance rate, the drift will be much larger at higher temperatures. However, due to exponential attenuation, the acceptance test of eq 6 is also less stringent, making the N(MC)^2 method more tolerant to the auxiliary potential. In practice, we found for the present DIM model that taking M as the number of atoms n gives a reasonably high (>90%) acceptance rate, thus wasting only a small fraction of the computing time in the sampling while gaining a large factor in the evaluation of the DIM energy. With respect to fully calculating the DIM energy by matrix diagonalization, the CPU gain in propagating the MC trajectory

dx.doi.org/10.1021/ct200846a | J. Chem. TheoryComput. 2012, 8, 639−648

with individual atomic moves on the perturbed energy surface amounts to a factor of 9.9 for Hg_{13} and 47 for Hg_{55}, which for a 90% acceptance rate back on the reference surface gives efficiency indices[67] of 9 and 42, respectively. Without such high numbers, the simulations would be short and limited to low cluster sizes, making phase transitions much harder to investigate computationally. Using $V_{pair}(\mathbf{R})$ as the approximate surface leads to much lower acceptance rates (below 25%, and below 10% at low temperature), which is not compensated by its lower computational cost.

In order to enhance convergence of the Monte Carlo simulation, we also combined the nested Markov chain MC with parallel tempering. This combination is straightforward and concerns the reference potential only. Various $N(MC)^2$ trajectories at different temperatures $T_j = 1/k_B\beta_j$ are now propagated in parallel, and occasionally the configurations $\mathbf{R}_i^{(j)}$ and $\mathbf{R}_i^{(j+1)}$ of adjacent trajectories j and $j+1$ attempt an exchange. This exchange is accepted on the basis of the Metropolis-like probability[58,59]

$$\begin{aligned} \mathrm{acc}(\mathbf{R}_i^{(j)} \rightleftharpoons \mathbf{R}_i^{(j+1)}) \\ = \min\{1, \exp[(\beta_j - \beta_{j+1})(V_{DIM}(\mathbf{R}_i^{(j)}) \\ - V_{DIM}(\mathbf{R}_i^{(j+1)}))]\} \end{aligned} \quad (7)$$

The parallel tempering method is of particular help at low temperatures, where high energy barriers may be difficult to cross. We have also considered exchanges between nonadjacent configurations,[68] without getting significantly faster convergence.

Random exchanges were attempted every 10 Monte Carlo cycles on the reference surface V_{DIM}, and a total of 32 trajectories were simulated in parallel. The number of total Monte Carlo steps was taken as 10^6 per replica, but the simulations were repeated by initializing each replica with the final configuration obtained at the previous run, until satisfactory convergence was reached. Finally, in order to circumvent the possible irreversible thermal dissociation of atoms at high temperatures, the clusters were enclosed in a hard-wall spherical container with radius R_c around their center of mass.

From the parallel tempering trajectories, and in addition to the averages of the DIM potential energy, the probability distributions of V_{DIM} were estimated and processed using the histogram reweighting method[69] into the caloric curves as a continuous function of temperature. We also evaluated the many-body component $\Delta E_{MB} = V_{DIM} - V_{pair}$ and its average. The Monte Carlo simulations were repeated for the pairwise potential V_{pair}, directly by parallel tempering and without any auxiliary potential, to yield the corresponding caloric curves.

3. STABLE STRUCTURES

The lowest-energy structures obtained for the DIM model using basin-hopping global optimization were analyzed using a variety of geometrical and energetic indicators. Besides symmetry considerations (point group), the binding energy E_{DIM} and the many-body contribution ΔE_{MB} were evaluated at the minimum energy of the DIM potential energy surface. These quantities are given in Table 1 for Hg_n clusters, $2 \le n \le 59$. It is important to notice that many global minima are highly symmetric, with many 5-fold and even 6-fold symmetry elements. Even minima with only a C_s point group,

Table 1. Total Binding Energy E_{DIM}, Many-Body Contribution $\Delta E_{MB} = E_{DIM} - E_{pair}$, and Point Group of the Global Minima of Hg_n Clusters, $2 \le n < 60$, As Obtained with the DIM Model

N	E_{DIM} (eV)	ΔE_{MB} (eV)	point group	N	E_{DIM} (eV)	ΔE_{MB} (eV)	point group
2	−0.050	0.000	$D_{\infty h}$	31	−6.840	0.172	C_s
3	−0.179	−0.031	D_{3h}	32	−7.086	0.254	C_{2v}
4	−0.415	−0.128	T_d	33	−7.308	0.248	C_s
5	−0.631	−0.194	D_{3h}	34	−7.541	0.378	D_{5h}
6	−0.880	−0.264	O_h	35	−7.773	0.369	C_2
7	−1.126	−0.322	D_{5h}	36	−7.984	0.421	C_1
8	−1.299	−0.324	C_s	37	−8.221	0.496	C_s
9	−1.553	−0.358	C_{2v}	38	−8.457	0.489	C_1
10	−1.791	−0.371	C_{3v}	39	−8.735	0.493	C_{6v}
11	−2.017	−0.368	C_{2v}	40	−8.966	0.604	D_{6h}
12	−2.307	−0.377	C_{5v}	41	−9.155	0.653	C_s
13	−2.683	−0.418	I_h	42	−9.384	0.662	C_1
14	−2.827	−0.379	C_{3v}	43	−9.666	0.717	C_s
15	−3.044	−0.365	C_{2v}	44	−9.879	0.783	C_1
16	−3.249	−0.335	C_s	45	−10.140	0.844	C_s
17	−3.470	−0.335	C_s	46	−10.361	0.872	C_s
18	−3.726	−0.305	C_s	47	−10.591	0.980	C_s
19	−4.065	−0.302	D_{5h}	48	−10.813	1.069	C_s
20	−4.251	−0.250	C_{2v}	49	−11.007	1.265	C_{3v}
21	−4.444	−0.212	C_1	50	−11.254	1.233	C_s
22	−4.687	−0.183	C_s	51	−11.503	1.411	C_{2v}
23	−5.002	−0.155	D_{3h}	52	−11.786	1.474	C_{3v}
24	−5.183	−0.103	C_{2v}	53	−12.061	1.547	S_{10}
25	−5.427	−0.125	C_{2v}	54	−12.335	1.621	C_{5v}
26	−5.703	−0.014	T_d	55	−12.610	1.694	I_h
27	−5.923	−0.006	C_{2v}	56	−12.780	1.752	C_{3v}
28	−6.122	0.067	C_s	57	−13.003	1.748	C_{2v}
29	−6.397	0.122	D_{3h}	58	−13.266	1.660	C_1
30	−6.616	0.133	C_{2v}	59	−13.567	1.701	C_s

such as the octamer or the 16-mer, are actually based on the pentagonal bipyramid or the icosahedron. A deviation from the 5-fold and 6-fold symmetries is found for the hexamer, which in agreement with other *ab initio* calculations[31] and recent dispersion-corrected DFT[36] studies is octahedral. Above this size, the growth pattern is that of Lennard-Jones clusters,[34,42,64] with maximum coordination until the first icosahedral shell is formed at $n = 13$. In particular, we do not find evidence for the elongated geometries reported for some sizes by Hartke and coworkers, who combined a genetic algorithm with a hybrid potential energy surface.[33] The binding energies vary strongly at small sizes, and more steadily with increasing number of atoms $n > 13$. The many-body contribution also increases with cluster size but changes sign at $n = 27$ and becomes repulsive above this size. Inspection of the nearest-neighbor distances, given as Supporting Information, reveals that many-body effects tend to contract bonds in the attractive regime and conversely lead to bond expansion once they become repulsive. While these geometrical and energetic features are consistent with each other, they are both rather unexpected, and we shall come back to them below in greater depth.

The growth pattern above size $n = 13$ is generally similar to that in Lennard-Jones clusters. Polyicosahedral shapes, in which the additional atoms maximize coordination with the underlying triangular faces in an anti-Mackay overlayer,[74] are found until $n = 48$. The multilayer icosahedra found above this size

and up to n = 55 adopt a more homogeneous radial packing with planar (111) faces, known as a Mackay overlayer. These two types of icosahedral packings were suggested decades ago from the interpretation of electron diffraction measurements,[75] and they have been discussed in greater detail by Northby,[74] and more recently by Wales and co-workers.[76]

However, there are also some differences with the structures that minimize V_{pair} in the absence of s−p mixing. The global minima obtained for Hg_n clusters described by the pairwise potential can also slightly differ from the LJ minima, as examplified by the octamer case, which is a doubly capped square bipyramid (C_{2v} point group) for the V_{pair} system, and a D_{5h} singly capped pentagonal bipyramid in the DIM model. However, the anti-Mackay to Mackay transition occurs at a comparable size for the two potentials. Factors affecting the anti-Mackay to Mackay transition include primarily the range of the potential,[70] as well as its anisotropy,[71] zero-point energies,[72] and the possibility of mixing different elements.[73] In the present case, the appearance of multilayer icosahedra is gradual and involves intermediate polyicosahedral packing with 6-fold symmetry elements, all features already present with the pairwise potential energy surface. In fact, the pairwise and many-body potential energy surfaces predict different global minima for about half of the sizes in the range $2 \leq n \leq 59$, but these differences are often minor atomic displacements from a common family. A selection of DIM global minima that differ from the pairwise global minima is given in Figure 1, all global minima being reported as Supporting Information. The minima of Figure 1 illustrate a variety of packing schemes encountered for mercury clusters in this size range.

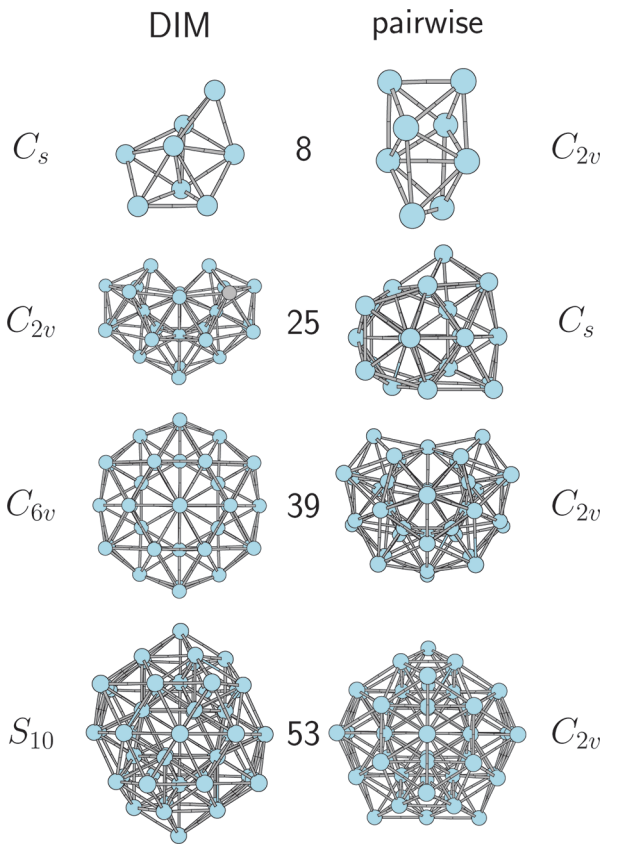

Figure 1. Selected global minima of mercury clusters obtained with the DIM model and with the pair Hg_2 potential, for sizes at which they differ from one another. The symmetries are also indicated.

The overall trend of the DIM model is to predict a slightly different polyicosahedral growth leading to the double icosahedron at n = 19 and to a triple icosahedron at n = 23, followed by oblate structures in the range 25−38. The other secondary magic numbers of polyicosahedral minima found in rare gas clusters at n = 26, 29, and 31, and which can be considered as entangled double icosahedra,[74] are not so prominent for mercury, but the energetic stabilities obtained with the DIM model agree nicely with those reported in ref 34. We also note that the truncated octahedral global minima found for n = 38 in Lennard-Jones clusters is destabilized both at the pairwise and DIM levels for mercury. This may be related to the destabilization of the cubic motif in bulk mercury, which adopts a rhombohedral crystalline structure. In this size range, a rather original feature takes place instead, as a 6-fold axis with maximum symmetry (D_{6h} point group) is reached at n = 40. The pairwise potential also finds this peculiar structure as its lowest-energy structure, indicating that it is not a specific many-body effect but rather a consequence of the ground state energy curve.

The 6-fold motif has been reported previously in binary metal clusters,[77] where it was interpreted as the manifestation of some release of surface strain to accommodate the competition among interactions between alike and unlike atoms. To the best of our knowledge, this motif has not been seen in homogeneous clusters until now, but its presence in the pairwise system suggests that it could be far more general in van der Waals clusters.

The completion of the two-layer icosahedron at n = 55 confirms that, with the present model, the directional effects of s−p mixing are still low in magnitude and that mercury clusters remain essentially bound by isotropic dispersive forces. Upon completion of the Mackay overlayer, additional atoms start to bind by maximizing coordination in an anti-Mackay fashion, as is observed in rare-gas clusters.[74] The greater stability of the anti-Mackay overlayer is confirmed in the size range $55 < n \leq 59$, where the global minima are distortions in their outer face with prominent pentagonal pyramids, in contrast with LJ clusters where the double icosahedron is preserved and simply capped.

Adding the zero-point vibrational correction at the harmonic level does not drastically change the binding energies, and the ordering between isomers is preserved for most cluster sizes. In particular, the polyicosahedral, 6-fold symmetric, and multilayer icosahedral structures are unaltered except for some details in the outer arrangements at nonmagic sizes.

The variations of the binding energy with the number of mercury atoms predicted by the DIM model and its pairwise approximation are both represented in Figure 2. Note that, in contrast with the data in Table 1, the pairwise energies correspond to the global optimization results obtained with the corresponding model, rather than single-point values V_{MB} at the minimum of the DIM potential energy surface. This figure also shows the energies obtained at the CCSD(T) level by Moyano and co-workers[34] for $n \leq 6$ and by Wang and co-workers[31] for n = 7. In the small sizes regime, the DIM approach agrees very satisfactorily with these electronic structure calculations. The energies found with the present implementation of the DIM model are also in quantitative correspondence with the original calculations of Kitamura,[37] despite our use of parametrized

dx.doi.org/10.1021/ct200846a | J. Chem. TheoryComput. 2012, 8, 639−648

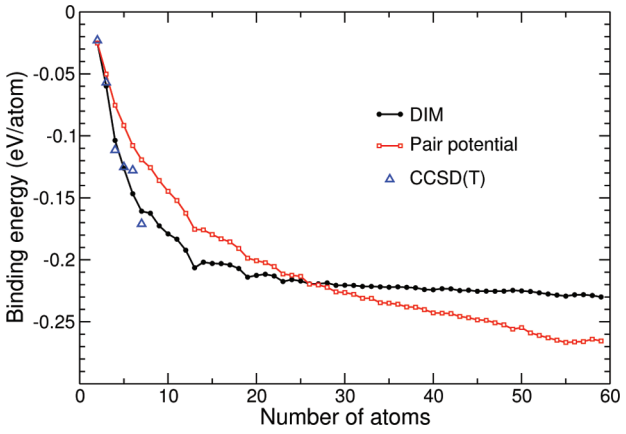

Figure 2. Binding energy per atom of the most stable structures of Hg_n clusters described with the many-body DIM model or with the pair potential. Additional *ab initio* results at the CCSD(T) level from ref 34 ($n \leq 6$) and from ref 31 ($n = 7$) are also indicated.

forms for the excited states curves and an updated ground state potential for Hg_2. The change in binding energy with the number of atoms also highlights the special stabilities found for the clusters containing 13, 19, and 23 atoms that belong to the polyicosahedral sequence, but the double-layer Mackay icosahedron at $n = 55$ is less remarkable.

Many-body effects, as given by the difference between the DIM and the pairwise models, are increasingly binding for the smallest clusters, but their contribution is stationary in the range $7 \leq n \leq 13$ before decreasing in magnitude and eventually becoming repulsive at around $n = 25$. This confirms the results of Table 1 and shows that it is not a consequence of incomplete atomic relaxation. The higher degree of mixing throughout the cluster may not thus be a simple function of coordination, as the original analysis by Kitamura would suggest[51] in his phenomenological application of the DIM model to fluid mercury. Although the experimental bulk limit for metallic Hg (0.67 eV, see ref 78) lies still far away for 50-atom clusters, it is unclear how the van der Waals to covalent and covalent to metallic transitions will affect variations in the size-dependent binding energy.[27−29,31,32] The evolution of the binding energy with increasing cluster size with the DIM model appears significantly slower than with the purely dispersive pairwise approximation, and a plot of these energies against $n^{-1/3}$ gives a cohesive energy of 0.27 eV below the experimental value. This could indicate that the appearance of metallic bonding is not correctly captured by the DIM model in large compounds, which would point to some specific deficiencies of this approach. Most likely, the term ξ introduced in the DIM matrix to empirically couple the $X^1\Sigma_g^+$ and $^1\Sigma_g^+$ states to each other may be appropriate under low coordination but could be improved through an *ab initio* determination of diatomics diabatic states. In bulk environments, it might undergo variations due to mixing of 6s6p states with higher excited states that are not accounted for in the present model. Extensions of the DIM approach in nonorthogonal schemes could also be considered.

4. MELTING BEHAVIOR

Contrary to bulk materials, atomic clusters melt gradually,[79] and the solid−liquid transition is usually shifted to lower temperatures due to the lower cohesion of surface atoms. Although the thermodynamics of metal clusters and nanoparticles has received sustained experimental attention for sodium[80,81] and aluminum,[82] not much is known for other metals. Two interesting exceptions relevant to this work are the cases of tin and gallium, where ion mobility measurements have indicated unexpectedly high melting points even higher than the bulk.[83,84] In the latter situation, this was interpreted as due to some bonding stabilization arising from a partially covalent character en route toward the metallic state.[85]

The present case of mercury is interesting in this respect, and the DIM model, despite some possible shortcomings identified above, could give some additional clues about the influence of many-body (covalent) effects on the melting temperature of weakly bound clusters.

Using nested Markov chain Monte Carlo combined with parallel tempering, we have simulated a few representative mercury clusters at finite temperatures and inferred the distributions of potential energies leading in turn to the caloric curves. In order to avoid specific size effects driven by particular structures, we have chosen to focus on Hg_{13}, Hg_{19}, and Hg_{55}, with container radii taken as $R_c = 6$, 7.5, and 10 Å, respectively. Again, all calculations were repeated for the pairwise model for comparison.

In addition to selected clusters, and in order to assess the performance of the DIM model for simulating bulk mercury and to unravel the importance of surface effects, we have carried out similar calculations for a periodic sample under constant zero pressure (NPT ensemble with $P = 0$) with rhombohedral boundary conditions treated in the minimum image convention. For a $5 \times 5 \times 5$ rhombohedral sample, the optimal parameters that minimize the crystal energy are found to be $a = 2.92$ Å for the lattice constant with an angle of $\alpha = 52°$, in reasonable agreement with the experimental values of 3.005 Å and 70.53°, respectively.[78] Note that we did not globally optimize the crystal structure for the DIM model, and more stable symmetries other than rhombohedral should not be ruled out. This 125-atom sample turned out to be too involved computationally, and we performed constant pressure simulations in a smaller box suited to the $4 \times 4 \times 4$ system, also employing the parallel tempering $N(MC)^2$ strategy, and with one volume move attempted after every 10 Monte Carlo cycles on the DIM potential energy surface.

The variations of the canonical heat capacities obtained for the DIM model and its pairwise approximation are represented in Figure 3 for the 13-, 19-, and 55-atom clusters and for the 64-atom sample with rhombohedral periodic boundary conditions under constant zero pressure. The configurational heat capacities are close to their ideal value of $1.5k_B$ at low and high temperatures and exhibit a broad peak indicative of a smooth solidlike−liquidlike transition over a range of about 100 K in the small clusters, reduced to about 50 K in Hg_{55}. The periodic sample shows a similar phenomenon, with a broadening of the transition due to finite size scaling effects of about 50 K as well. More interestingly, the transition temperatures indicated by the maximum of the peak steadily *decrease* with increasing cluster size from 245 K (Hg_{13}) to 235 K (Hg_{19}) and 160 K (Hg_{55}), a rather counterintuitive feature, which suggests that s−p mixing destabilizes the solidlike state. The bulk system displays a melting temperature close to 250 K, in surprisingly good agreement with experimental results (234.32 K) considering the inherent approximations of the DIM model. The broadening of ca. 50 K is here due to a finite box effect.

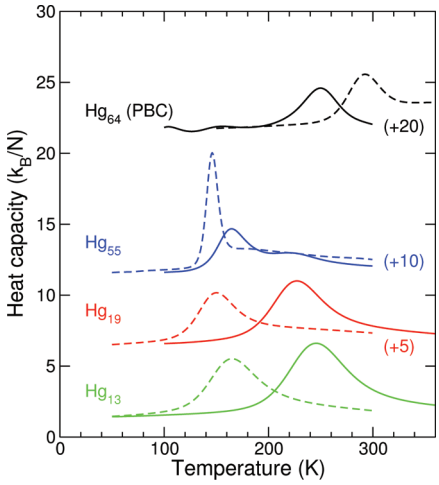

Figure 3. Canonical heat capacities of mercury clusters (at constant volume) and a bulk sample (at zero pressure, with periodic boundary conditions—PBC), as a function of temperature. Results for the many-body DIM model and the pair potential are shown as solid and dashed lines, respectively. For clarity, some curves have been vertically shifted by an amount of k_B/N indicated between parentheses.

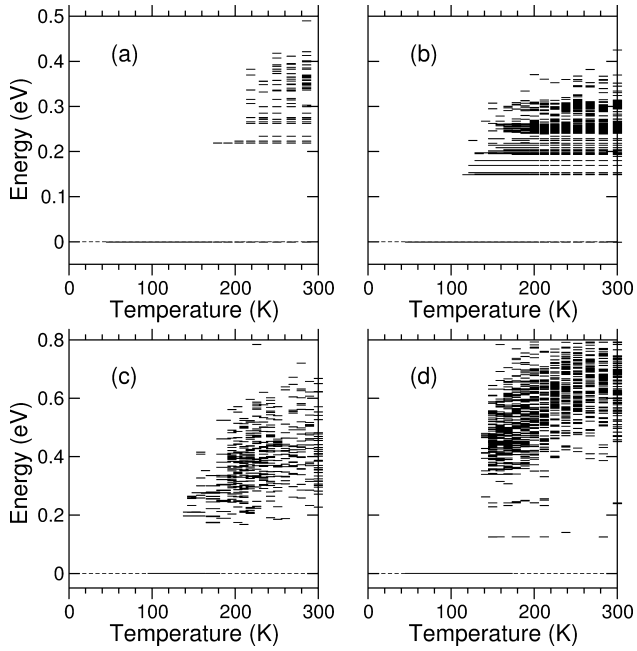

Figure 4. Spectra of isomer energies sampled during the Monte Carlo simulations, for (a and b) Hg_{13} and (c and d) Hg_{55}. Results in panels a and c are for the many-body DIM model; panels b and d are for the pair potential. All energies are relative to the corresponding global minimum.

Inspection of the caloric curves obtained for the corresponding clusters bound by the pairwise model reveals very similar heat capacity peaks, only shifted to lower melting temperatures of about 140−160 K. Finite size effects are lower on the melting temperatures but more significant on the broadening of the phase change, the melting peak obtained for Hg_{55} being much sharper than in the DIM description. This feature is associated with a higher latent heat of fusion, which itself is likely related to a greater energy gap between the solid and liquid states. In contrast with clusters, the neglect of many-body effects in the bulk system significantly enhances the melting temperature by about 20%, or 40 K, without influencing much the latent heat or broadening of the transition.

For the systems considered here, clusters modeled with the pair potential roughly behave like conventional Lennard-Jones clusters, with essentially no size dependence of the melting temperature until 55 atoms are reached, and a much higher melting temperature for the bulk. The presence of s−p mixing drastically changes this picture, giving rise to strong many-body effects already above 19 atoms. The change in the melting point upon neglecting s−p mixing also suggests different relative stabilities of the solidlike and liquidlike isomers. This property can be analyzed from an inherent structure perspective,[86] in which the configurations recorded during the Monte Carlo trajectories are locally minimized into their closest stable structure. At a given temperature, the set (or spectrum) of isomer energies indicates which inherent structures of the landscape are effectively sampled.[87] By representing the spectrum as a function of increasing temperature, qualitative changes act as the fingerprints of the collective phase changes.[55] Unfortunately, this approach is less straightforward in the case of the bulk system under constant pressure, because the isomer energy depends on the density, which varies across the NPT simulation.

The spectra of isomers obtained for Hg_{13} and Hg_{55} by systematic quenching are represented in Figure 4, and in each case the inherent structure analysis was performed for the DIM and pairwise models. In all cases, the solidlike state is associated with a single, well-defined minimum while the liquidlike state is composed of a large number of "excited" minima separated by a significant energy gap, corresponding here to the formation of a single-atom defect at the surface of the icosahedra. These higher-lying minima appear near 200 and 120 K for Hg_{13} in the DIM and pairwise models, respectively, and near 150 K for Hg_{55} for both descriptions. These values agree well with the temperatures at which the heat capacities reach their maxima in Figure 3. The energy gap between the solid and liquid isomers is an important part of the latent heat of fusion, but the more extended range of excited isomers found in the pairwise model for Hg_{55} also explains the higher peak obtained for this system. The energy gap between low-lying isomers also contributes to the melting temperature itself, as it measures the amount of thermal energy needed to populate these other isomers. In the DIM approach, this gap is close to 0.2 eV or more, whereas the pairwise approximation yields values closer to 0.1−0.15 eV. This increase of the energy needed to create defects due to many-body effects is thus consistent with the higher melting point found in the Monte Carlo simulations.

We have finally considered the influence of a finite temperature on the many-body contribution V_{MB} to the binding energy. The thermal average $\langle V_{MB} \rangle$ was calculated along the Monte Carlo simulations, and its variations with temperature are represented in Figure 5 for Hg_{13} and Hg_{55}. For these cluster sizes and at $T = 0$, s−p mixing in the DIM approach changes from being cohesive ($n = 13$) to being repulsive ($n = 55$). Temperature effects do not alter this picture, but thermal fluctuations tend to decrease the magnitude of many-body effects, especially as the melting point is crossed. We expect many-body effects to be reduced in the lower-density fluid phases relative to the solid state, which precisely explains why pair potentials seem to work for liquid Hg.[5−7] This is consistent with Figure 5, and this encouraging

dx.doi.org/10.1021/ct200846a | J. Chem. TheoryComput. 2012, 8, 639−648

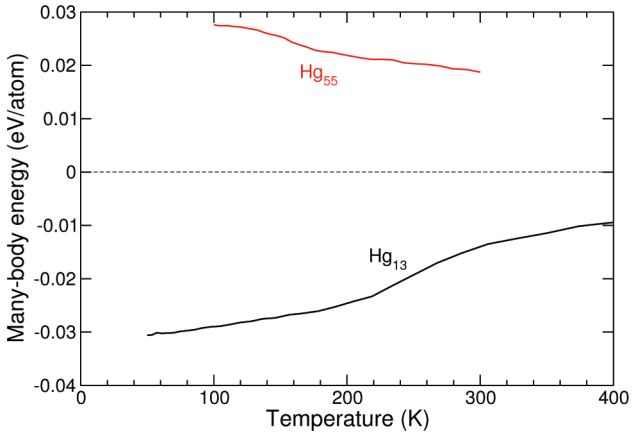

Figure 5. Thermally averaged many-body energy as a function of temperature for the Hg_{13} and Hg_{55} clusters, as obtained from histogram-reweighted Monte Carlo simulations.

result motivates the use of the DIM model to address the fluid states of bulk mercury.

5. DISCUSSION AND CONCLUSION

Changes in chemical bonding due to increasing number of atoms are by nature a complex many-body effect, which cannot be represented by conventional explicit interatomic potentials. In the case of mercury, the slow convergence of the many-body expansion of the binding energy[41,42] is a strong drawback for establishing practical and accurate models for statistical simulations. On the other hand, popular electronic structure methods able to handle large systems are currently limited to density-functional theory, and at present the accuracy of DFT for mercury remains questionable.[42,43]

Alternative quantum chemical methods are thus desirable to calculate the properties of large mercury compounds at finite temperature. A very promising approach, motived by some *ab initio* investigations,[41,42] and already used in the past to describe barium clusters,[44] consists of complementing a Hartree−Fock calculation by a pairwise approximation of the electronic correlation energy. Although some work is still required for the method to be applied routinely for reasonably large and disordered systems, it can be hoped to provide in the near future an accurate reference potential energy surface for mercury clusters accross the insulating, semiconducting, and metallic regimes.

In anticipation, we have explored a simple quantum model based on the diatomics-in-molecule approach, in which the mixing effects between 6p and 6s orbitals are included in a CI fashion. The model, built for mercury along the original lines of Kitamura,[45] was slightly upgraded by considering a more recent potential energy curve for the Hg dimer.[62] Due to the diagonalization step, the computational cost of the DIM approach does not scale favorably with size, and for large systems the sparsity of the Hamiltonian matrix could probably be exploited in linear scaling schemes. However, in the context of Monte Carlo sampling, we have found it extremely useful to approximate the full DIM potential energy surface by its first-order perturbation representation with respect to a reference state. The nested Markov chain MC scheme, here combined with parallel tempering, is a powerful method for statistical sampling purposes with few and well-controlled parameters.

Compared with available reference *ab initio* data, the DIM model is energetically accurate for small clusters. The stable structures of mercury clusters predicted by the model generally display similar patterns as rare-gas clusters, with icosahedral motifs and pentagonal symmetry. The main differences with the rare gases include a favored polyicosahedral growth, some unusual 6-fold symmetry elements, none of them being strict consequences of many-body mixing effects. The finite-temperature thermodynamics, on the other hand, shows surprising features with the DIM model, with a melting temperature that decreases with increasing size in small clusters. In contrast, clusters modeled with the pairwise potential display size effects that are very similar to those found in Lennard-Jones clusters.

The many-body effects and s−p orbital mixing predicted by the DIM model were found to be attractive at small sizes but repulsive above a few tens of atoms. While this may be a true signature of the growing importance of covalent character, it is not compatible with the expected strengthening of the chemical bond. The cohesion energies, in particular, are too low in large clusters, and this may point at a deficiency of the model, which perhaps could be cured in the rather empirical way mixing is introduced in the matrix elements. One notable outcome of this observation is that the extrapolation attempted by Kitamura to relate many-body effects to coordination and bond distances[51] may be oversimplified. Extensions of the DIM approach could include higher excited states and the contribution of states dissociating asymptotically into ionic fragments. Indeed, additional states with charge transfer, ignored in the current model, could also be considered, especially in concern with the nonmetal to metal transition. However, these extensions would significantly enlarge the Hamiltonian matrix and lead to a major extra computational burden.

Subsequent efforts should be aimed at validating or refining the DIM model by means of the Hartree−Fock + pair correlation approach, or by dispersion-corrected density functional theory. This would enable the use of this model as the approximate potential for exploring the energy landscapes more efficiently in hierarchical global optimization or in the context of nested Markov chain Monte Carlo. Nonrelativistic versions of the model, in which the DIM model is constructed from nonrelativistic *ab initio* ingredients and without spin−orbit coupling, could then contribute to elucidating the role of relativity on the peculiar thermodynamical properties of mercury from the atomistic point of view.

■ ASSOCIATED CONTENT

Supporting Information

Pictures of all global minima in the size range $3 \leq n \leq 59$, number of nearest-neighbor contacts, and average bond length. This material is available free of charge via the Internet at http://pubs.acs.org.

■ AUTHOR INFORMATION

Corresponding Author

*E-mail: fcalvo@lasim.univ-lyon1.fr.

Notes

The authors declare no competing financial interest.

■ ACKNOWLEDGMENTS

We acknowledge financial support from PHC Dumont D'Urville (Project 23764SC). Some computational resources were provided by the regional Pôle Scientifique de Modélisation Numérique, which is gratefully acknowledged. P.S. is

grateful to the Alexander von Humboldt Fundation for financial support.

REFERENCES

(1) Pahl, E.; Schwerdtfeger, P. In *Handbook of Nanophysics. Clusters and Fullerenes*; Sattler, K. D., Ed.; CRC Press: Boca Raton, FL, 2010.
(2) Singh, P. P. *Phys. Rev. Lett.* **1994**, *72*, 2446.
(3) Kozhevnikov, V.; Arnold, D.; Grodzinskii, E.; Naurzakov, S. *J. Non-Cryst. Solids* **1996**, *205*, 256.
(4) Inui, M.; Hong, X.; Tamura, K. *Phys. Rev. B* **2003**, *68*, 094108.
(5) Raabe, G.; Sadus, R. J. *J. Chem. Phys.* **2003**, *119*, 6691.
(6) Tóth, G. *J. Chem. Phys.* **2003**, *118*, 3949.
(7) Bomont, J.-M.; Bretonnet, J.-L. *J. Chem. Phys.* **2006**, *124*, 054504.
(8) Yao, M.; Uchtmann, H.; Hensel, F. *Surf. Sci.* **1985**, *156*, 465.
(9) Uchtmann, H.; Dettmer, R.; Baranovskii, S. D.; Hensel, F. *J. Chem. Phys.* **1998**, *108*, 9775.
(10) von Issendorff, B.; Cheshnovsky, O. *Annu. Rev. Phys. Chem.* **2005**, *56*, 549.
(11) Bréchignac, C.; Broyer, M.; Cahuzac, Ph.; Delacretaz, G.; Labastie, P.; Wöste, L. *Chem. Phys. Lett.* **1985**, *120*, 559.
(12) Bréchignac, C.; Broyer, M.; Cahuzac, Ph.; Delacretaz, G.; Labastie, P.; Wolf, J. P.; Wöste, L. *Phys. Rev. Lett.* **1988**, *60*, 275.
(13) Haberland, H.; Kornmeier, H.; Langosch, H.; Oschwald, M.; Tanner, G. *J. Chem. Soc., Faraday Trans.* **1990**, *86*, 2473.
(14) Rademann, K.; Dimopoulou-Rademann, O.; Schlauf, M.; Even, U.; Hensel, F. *Phys. Rev. Lett.* **1992**, *69*, 3208.
(15) Kaiser, B.; Rademann, K. *Phys. Rev. Lett.* **1992**, *69*, 3204.
(16) Busani, R.; Folkers, M.; Cheshnovsky, O. *Phys. Rev. Lett.* **1998**, *81*, 3836.
(17) Blanc, J.; Broyer, M.; Dugourd, Ph.; Labastie, P.; Sence, M.; Wolf, J. P.; Wöste, L. *J. Chem. Phys.* **1995**, *102*, 680.
(18) Bréchignac, C.; Broyer, M.; Cahuzac, Ph.; Delacretaz, G.; Labastie, P.; Wöste, L. *Chem. Phys. Lett.* **1985**, *118*, 174.
(19) Ito, H.; Sakurai, T.; Matsuo, T.; Ichihara, T.; Katakuse, I. *Z. Phys. D: At. Mol. Clusters* **1997**, *40*, 102.
(20) Bescós, B.; Lang, B.; Weiner, J.; Weiss, V.; Viedenmann, E.; Gerber, G. *Eur. Phys. J. D* **1999**, *9*, 399.
(21) Verlet, J. R. R.; Bragg, A. E.; Kammrath, A.; Cheshnovsky, O.; Neumark, D. M. *J. Chem. Phys.* **2004**, *121*, 10015.
(22) Griuffin, G. B.; Ehrier, O. T.; Kammrath, A.; Young, R. M.; Cheshnovsky, O.; Neumark, D. M. *J. Chem. Phys.* **2009**, *130*, 231103.
(23) Jank, W.; Hafner, J. *Phys. Rev. B* **1990**, *42*, 4926.
(24) González, L. E.; González, D. J.; Calderín, L.; Şengül, S. *J. Chem. Phys.* **2008**, *129*, 171103.
(25) Paulus, B.; Rosciszewski, K. *Chem. Phys. Lett.* **2004**, *394*, 96.
(26) Zaleski-Ejgierd, P. K.; Pyykkö, P. *Phys. Chem. Chem. Phys.* **2011**, *13*, 16510.
(27) Pastor, G. M.; Stampfli, P.; Bennemann, K. H. *Phase Trans.* **1990**, *24*−*6*, 371. Pastor, G. M.; Stampfli, P.; Bennemann, K. H. *Europhys. Lett.* **1988**, *7*, 419.
(28) Ohnishi, S.; Ishii, Y. *Z. Phys. D: At. Mol. Clusters* **1993**, *26*, S143.
(29) Zhao, J. J.; Chen, X. S.; Wang, G. H. *Austr. J. Phys.* **1995**, *48*, 731.
(30) Dolg, M.; Flad, H.-J. *Mol. Phys.* **1997**, *91*, 815.
(31) Wang, Y. X.; Field, H. J.; Dolg, M. *Int. J. Mass Spectrom.* **2000**, *201*, 196.
(32) Tomilin, O. B.; Akamova, L. V.; Yudin, P. A.; Terekhin, I. I. *J. Struct. Chem.* **2001**, *42*, 519.
(33) Hartke, B.; Flad, H.-J.; Dolg, M. *Phys. Chem. Chem. Phys.* **2001**, *3*, 5121.
(34) Moyano, G. E.; Wesendrup, R.; Söhnel, T.; Schwerdtfeger, P. *Phys. Rev. Lett.* **2002**, *89*, 103401.
(35) Kang, J.; Kim, J.; Ihee, H.; Lee, Y. S. *J. Phys. Chem. A* **2010**, *114*, 5630.
(36) Fernández, E. M.; Balbás, L. C. *Phys. Chem. Chem. Phys.* **2011**, *13*, 20863.
(37) Kitamura, H. *Chem. Phys. Lett.* **2007**, *425*, 205. Kitamura, H. *Eur. Phys. J. D* **2007**, *43*, 33.
(38) Pyykkö, P. *Adv. Quantum Chem.* **1978**, *11*, 353. Pyykkö, P. *Chem. Rev.* **1988**, *88*, 563.
(39) Singh, P. P. *Phys. Rev. B* **1994**, *49*, 4954.
(40) Patil, H. *J. Chem. Phys.* **1991**, *94*, 3586.
(41) Paulus, B.; Rosciszewski, K.; Gaston, N.; Schwerdtfeger, P.; Stoll, H. *Phys. Rev. B* **2004**, *70*, 165106.
(42) Gaston, N.; Schwerdtfeger, P. *Phys. Rev. B* **2006**, *74*, 024105.
(43) Biering, S.; Schwerdtfeger, P. *Theor. Chem. Acc.* **2011**, *130*, 455.
(44) Boutou, V.; Allouche, A. R.; Spiegelmann, F.; Chevaleyre, J.; Aubert-Frécon, M. *Eur. Phys. J. D* **1998**, *2*, 63.
(45) Kitamura, H. *Chem. Phys.* **2006**, *325*, 207.
(46) Pfeiffer, G. V.; Huff, N. T.; Greenawalt, E. M.; Ellison, F. O. *J. Chem. Phys.* **1967**, *46*, 821.
(47) Steiner, E.; Certain, P. R.; Kuntz, P. J. *J. Chem. Phys.* **1973**, *59*, 47.
(48) Eaker, C. W. *J. Chem. Phys.* **1978**, *69*, 1453.
(49) Schreiber, J. L.; Kuntz, P. J. *J. Chem. Phys.* **1982**, *76*, 1872. Kuntz, P. J.; Schreiber, J. L. *J. Chem. Phys.* **1982**, *76*, 4120.
(50) Olson, J. A.; Garrison, B. J. *J. Chem. Phys.* **1984**, *81*, 1355.
(51) Kitamura, H. *J. Phys. Cond. Matter* **2007**, *19*, 072102. Kitamura, H. *J. Chem. Phys.* **2007**, *126*, 134509.
(52) Pahl, E.; Calvo, F.; Koçi, L.; Schwerdtfeger, P. *Angew. Chem., Int. Ed.* **2008**, *47*, 8207.
(53) Buffat, Ph.; Borel, J.-P. *Phys. Rev. A* **1976**, *13*, 2287.
(54) Lai, S. L.; Guo, J. Y.; Petrova, V.; Ramanath, G.; Allen, L. H. *Phys. Rev. Lett.* **1996**, *77*, 99.
(55) Calvo, F.; Spiegelmann, F. *J. Chem. Phys.* **2000**, *112*, 2888.
(56) Iftimie, R.; Salahub, D.; Wei, D.; Schofield, J. *J. Chem. Phys.* **2009**, *130*, 164104.
(57) Gelb, L. D. *J. Chem. Phys.* **2003**, *118*, 7747.
(58) Swendsen, R. H.; Wang, J.-S. *Phys. Rev. Lett.* **1986**, *57*, 2607.
(59) Geyer, C. J. In *Computing Science and Statistics: Proceedings of the 23rd Symposium on the Interface*; Keramidas, E. K., Ed.; Interface Foundation: Fairfax Station, VA, 1991; p 156.
(60) Cohen, J. S.; Schneider, B. *J. Chem. Phys.* **1974**, *61*, 3230.
(61) Czuchaj, E.; Rebentrost, F.; Stoll, H.; Preuss, H. *Chem. Phys.* **1997**, *214*, 277.
(62) Pahl, E.; Figgen, D.; Thierfelder, C.; Peterson, K. A.; Calvo, F.; Schwerdtfeger, P. *J. Chem. Phys.* **2010**, *132*, 114301.
(63) Li, Z.; Scheraga, H. A. *Proc. Natl. Acad. Sci. U.S.A.* **1987**, *84*, 6611.
(64) Wales, D. J.; Doye, J. P. K *J. Phys. Chem. A* **1997**, *101*, 5111.
(65) Hartke, B. *J. Phys. Chem.* **1993**, *97*, 9973. Calvo, F.; Tran, S.; Blundell, S. A.; Guet, C.; Spiegelmann, F. *Phys. Rev. B* **2000**, *62*, 10394.
(66) Coe, J. D.; Sewell, T. D.; Shaw, M. S. *J. Chem. Phys.* **2009**, *130*, 164104.
(67) Calvo, F. *Int. J. Quantum Chem.* **2010**, *110*, 2347.
(68) Calvo, F. *J. Chem. Phys.* **2005**, *123*, 124106.
(69) Ferrenberg, A. M.; Swendsen, R. H. *Phys. Rev. Lett.* **1988**, *61*, 2635. Ferrenberg, A. M.; Swendsen, R. H. *Phys. Rev. Lett.* **1989**, *63*, 1195.
(70) Doye, J. P. K; Berry, R. S.; Wales, D. J. *J. Chem. Phys.* **1995**, *103*, 4234.
(71) Calvo, F.; Boutin, A.; Labastie, P. *Eur. Phys. J. D* **1999**, *9*, 189.
(72) Calvo, F.; Doye, J. P. K; Wales, D. J. *J. Chem. Phys.* **2001**, *114*, 7312.
(73) Calvo, F.; Yurtsever, E. *Phys. Rev. B* **2004**, *70*, 045423.
(74) Northby, J. A. *J. Chem. Phys.* **1987**, *87*, 6166.
(75) Farges, J.; de Feraudy, M.-F.; Raoult, B.; Torchet, G. *J. Chem. Phys.* **1983**, *78*, 5067. Farges, J.; de Feraudy, M.-F.; Raoult, B.; Torchet, G. *J. Chem. Phys.* **1986**, *84*, 3491.
(76) Wales, D. J.; Doye, J. P. K; Miller, M. A.; Mortenson, P. N.; Walsh, T. R. *Adv. Chem. Phys.* **2000**, *115*, 1.
(77) Aprà, R.; Baletto, F.; Ferrando, R.; Fortunelli, A. *Phys. Rev. Lett.* **2004**, *93*, 065502.
(78) Lide, D. R. *CRC Handbook of Chemistry and Physics*; CRC Press: Boca Raton, FL, 2008.
(79) Aguado, A.; Jarrold, M. F. *Annu. Rev. Phys. Chem.* **2011**, *62*, 151.

(80) Martin, T. P.; Näher, U.; Schaber, H.; Zimmermann, U. *J. Chem. Phys.* **1994**, *100*, 2322.
(81) Schmidt, M.; Kusche, R.; Kronmüller, W.; von Issendorff, B.; Haberland, H. *Phys. Rev. Lett.* **1997**, *79*, 99.
(82) Breaux, G. A.; Neal, C. M.; Cao, B.; Jarrold, M. F. *Phys. Rev. Lett.* **2005**, *94*, 173401.
(83) Shvartsburg, A. A.; Jarrold, M. F. *Phys. Rev. Lett.* **2000**, *85*, 2530.
(84) Breaux, G. A.; Benirschke, R. C.; Sugai, T.; Kinnear, B. S.; Jarrold, M. F. *Phys. Rev. Lett.* **2003**, *91*, 215508.
(85) Chacko, S.; Joshi, K.; Kanhere, D. G.; Blundell, S. A. *Phys. Rev. Lett.* **2004**, *92*, 135506.
(86) Stillinger, F. H.; Weber, T. A. *Phys. Rev. A* **1982**, *25*, 978.
(87) Calvo, F.; Spiegelman, F. *Phys. Rev. Lett.* **1999**, *82*, 2270.